Spin-orbit torque in a Ni-Fe single layer

Takeshi Seki [1,2,*] Yong-Chang Lau [1,2] Satoshi Iihama [3,2,5] and Koki Takanashi [1,2,4]

[1] *Institute for Materials Research, Tohoku University, Sendai 980-8577, Japan*

[2] *Center for Spintronics Research Network, Tohoku University, Sendai 980-8577, Japan*

[3] *Frontier Research Institute for Interdisciplinary Sciences, Tohoku University, Sendai 980-8578, Japan*

[4] *Center for Science and Innovation in Spintronics, Core Research Cluster, Tohoku University, Sendai 980-8577, Japan*

[5] *WPI Advanced Institute for Materials Research, Tohoku University, Sendai 980-8577, Japan*

(Received 30 April 2021; revised 3 September 2021; accepted 9 September 2021; published 24 September 2021)

We evaluated the self-induced spin-orbit torque (SOT) in a single ferromagnetic layer. Spin-torque ferromagnetic resonance (ST-FMR) was measured for the very thin Ni-Fe (permalloy, Py) layers with and without structural inversion symmetry: *asymmetric* and *symmetric* Py layers. For both structures, the fieldlike component coming from the Oersted field clearly appeared. On the other hand, the dampinglike component was observed only for asymmetric Py with thickness $\leqslant 3$ nm. This dampinglike torque is attributable to the significant spatial change in the properties of Py. We propose a toy model to analyze the self-induced SOT.

DOI: 10.1103/PhysRevB.104.094430

Spin Hall effect (SHE) is the most promising way to convert from charge current (J_c) to spin current (J_s) and has been studied in a variety of nonmagnets (NMs) [1]. Exploiting the SHE-induced J_s, one can make a torque acting on the local spin of a ferromagnet (FM), which is called spin-orbit torque (SOT) [2]. The structure frequently used for SOT experiments is a NM/FM bilayer [2–8]. It had been believed that the nonmagnetic layer is essential to generate SOT acting on the ferromagnetic layer. However, after the pioneering works on the conversion from J_s to J_c in a FM [9–11], charge-spin conversion was reported for many kinds of FMs [12–31], and it has recently been revealed that SOT generated in a FM can switch the magnetization of the FM itself [32,33].

Representative works on SOT in a single FM were done for $L1_0$-FePt [32–35], disordered CoPt [36,37], Fe-Mn [38,39], Co-Tb [40], and Ni-Fe (permalloy, Py) [41]. In addition to the observation of SOT switching in the single ferromagnetic layer, spin-torque oscillation in the Py single layer [42] has been demonstrated, which enlarged an avenue for SOT-based device applications. On the whole, thick ferromagnetic layers, e.g., a CoPt layer with thickness of $\geqslant 8$ nm [36], were necessary to generate SOT. Several scenarios have been proposed, and a plausible explanation is that the spatial inversion symmetry breaking due to the composition or the disorder gradient plays an essential role in generating SOT [32,33]. On the other hand, some works claimed no detectable long-range asymmetry in the ferromagnetic layer [36]. Thus, the mechanism of SOT in the single FM is under debate, and it is indispensable to carry out a systematic study using a conventional spintronic material such as thin Py.

Let us organize what possible sources of broken inversion symmetry exist along the normal direction to the film plane, which is the essential question for the observation of SOT in a single FM. Given two different nonmagnetic materials of NM1 and NM2, (i) an asymmetric NM1/FM/NM2 structure breaks the inversion symmetry. Also, (ii) a NM1/FM/NM1 structure can be inversion asymmetric if the NM1/Py and Py/NM1 interfaces are not equivalent. In addition, (iii) within the FM layer itself, microstructure evolution such as composition gradient can break the inversion symmetry. In order to separate those possible sources, it is a straightforward way to evaluate SOT for both symmetric and asymmetric FMs with various layer thicknesses.

In this paper, we report the spin-torque ferromagnetic resonance (ST-FMR) for very thin Py layer devices with and without structural inversion symmetry: *asymmetric* and *symmetric* Py. The dampinglike and fieldlike components of SOT were evaluated together with the magnetic Gilbert damping parameter for the Py layers with various thicknesses (d). We show that dampinglike SOT becomes remarkable for the asymmetric Py samples as d is reduced to 1.5 nm. A toy model to analyze self-induced SOT is also proposed.

Thin films were prepared on a thermally oxidized Si (Si-O) substrate by employing an ion beam sputtering system. The base pressure was of the order of 10^{-5} Pa, and the deposition temperature was room temperature. The composition of Py was determined to be $Ni_{81}Fe_{19}$ by electron probe x-ray microanalysis. As schematically illustrated in Fig. 1(a), the asymmetric Py samples (Asym-Py) have the film stack of Si-O Subs.//Py(d)/Al-O(5) (in nanometers), in which d was varied in the range from 1.0 to 15.0 nm, while the symmetric Py samples (Sym-Py) are composed of Si-O Subs.//Al-O(5)/Py(d)/Al-O(5). The layer thicknesses were controlled using the sputter-deposition rates estimated prior to the sample preparation. In addition, two kinds of Py/Pt samples, Si-O Subs.//Py(5)/Pt(5)/Al-O(5) and Si-O Subs.//Pt(5)/Py(5)/Al-O(5), were prepared as reference samples. Magnetic properties were measured at room temperature using a superconducting quantum interference device

*takeshi.seki@tohoku.ac.jp

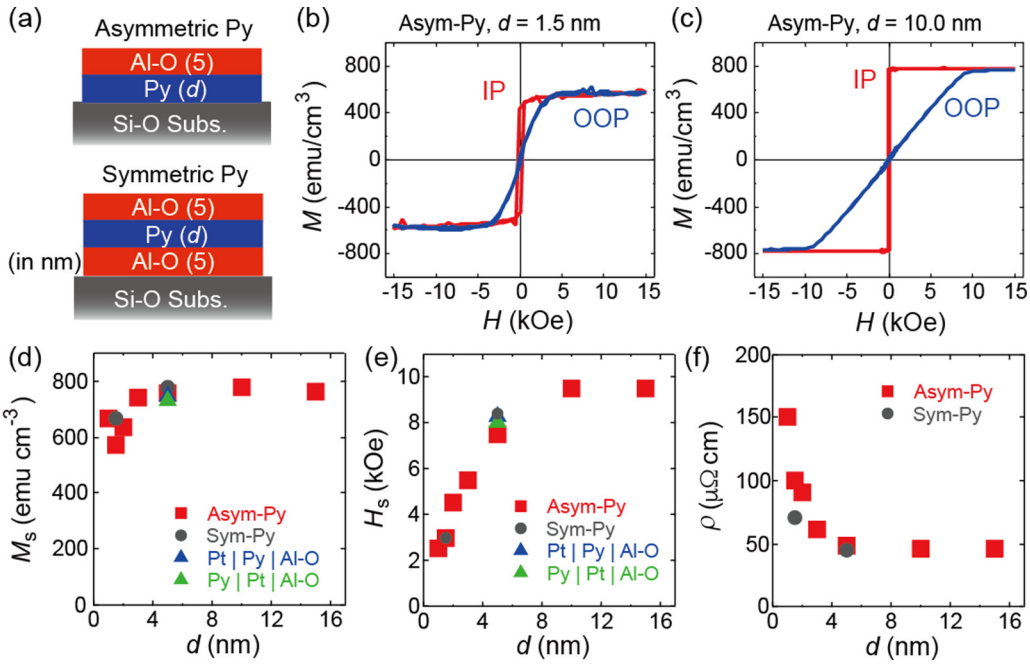

FIG. 1. (a) Schematic illustration of thin Ni-Fe (permalloy, Py) layers with and without structural inversion symmetry, which are called asymmetric Py (Asym-Py) and symmetric Py (Sym-Py). (b) Magnetization curves for Asym-Py with the Py layer thicknesses (d) of 1.5 nm and (c) 10.0 nm. The magnetic field (H) was applied along the out-of-plane (OOP) and in-plane (IP) directions, which are represented by the blue and red curves, respectively. (d) Saturation magnetization (M_s), (e) saturation field (H_s), and (f) resistivity (ρ) as a function of d. The red squares, gray circles, and triangles denote the data of Asym-Py, Sym-Py, and the Pt/Py reference samples, respectively.

magnetometer. Figures 1(b) and 1(c) display the magnetization curves for Asym-Py with $d = 1.5$ and 10.0 nm, respectively. The blue and red curves denote the magnetization curves with the external magnetic field (H) applied along the out-of-plane (OOP) and in-plane (IP) directions, respectively. Figures 1(d) and 1(e) plot the d dependence of saturation magnetization (M_s) and the saturation field along the OOP direction (H_s), respectively, for Asym-Py, Sym-Py, and the Py/Pt references. Here, M_s is reduced with decreasing d, suggesting the presence of a magnetic dead layer, and no definite film stack dependence is observed for $d = 5$ nm. Similarly, regardless of the film stacks, H_s shows a clear reduction as d is decreased. It is noted that the change in the demagnetizing field $4\pi M_s$ fails to fully explain the d dependence of H_s, implying the contribution of perpendicular magnetic anisotropy induced at the interfaces. The resistivity (ρ) of the Py layer rapidly increases for the low d samples, as shown in Fig. 1(f), which can be attributed to the effect of interface scattering and/or the change in the film morphology.

For the ST-FMR measurement, the films were patterned into a rectangular-shaped element with 10 μm width and 40 μm length, and the Au electrodes were made to form the coplanar waveguide shape using photolithography and Ar ion milling. As illustrated in Fig. 2(a), the ST-FMR was measured by applying the radiofrequency (RF) current (I_{rf}) along the x direction. The RF power of 15 dBm with the fixed frequency (f) was applied from a signal generator. Even in the case of a Py single-layer device, an oscillating transverse magnetic field (H_{rf}) could be induced in the y direction, as explained later. When H matched the resonance field (H_R), the device resistance [$R(t)$] oscillated through the anisotropic magnetoresistance (AMR) effect. As a result, applied $I_{rf}(t)$ [$= I\cos(2\pi ft)$] and oscillating $R(t)$ [$\propto \cos(2\pi ft)$] generated a rectification direct current (DC) voltage (V_{dc}), which was detected by a lock-in amplifier. All the ST-FMR measurements were carried out at room temperature. Figures 2(b)–2(e) display the V_{dc} as a function of H for Asym-Py with $d = 5.0$, 3.0, 2.0, and 1.5 nm, respectively. Here, f was set at 7 GHz, and H was applied at the in-plane angle (θ) of 45°, in which the Py magnetization vector (**m**) follows the direction of **H**. As reported in Ref. [3], the spectra of V_{dc} were fitted using the summation of Lorentzian and anti-Lorentzian functions given by $V_{dc} = V_L(\theta)f_L(H) + V_{AL}(\theta)f_{AL}(H)$, respectively, in which $f_L(H) = (\Delta H/2)^2/[(H_R - H)^2 + (\Delta H/2)^2]$ and $f_{AL}(H) = (\Delta H/2)(H_R - H)/[(H_R - H)^2 + (\Delta H/2)^2]$, and ΔH represents the resonance linewidth. Here, V_L is proportional to the dampinglike torque (τ_X^0), where V_{AL} is proportional to the fieldlike torque (τ_Y^0) including the Oersted field contribution. For $d = 5.0$ nm, the spectral shape is well fitted only by the anti-Lorentzian function, indicating no V_L component. As d is reduced, however, the V_L component becomes nonnegligible. For $d = 1.5$ nm, the V_L component is observed remarkably.

The θ dependence of V_{AL} and V_L for Asym-Py with $d = 1.5$ nm is plotted in Fig. 3(a), where f was set at 7 GHz. The current-induced Oersted field torque (τ_{Oe}) is generally a major source of τ_Y^0. Given the field angular dependence of resistance change (ΔR) via the AMR, $\Delta R \cdot \tau_{Oe}$ can be described by the $\sin2\theta\cos\theta$ function. On the other hand, if τ_X^0 mainly comes from the SHE, the combination of spin Hall torque (τ_{SH}) and ΔR also shows the $\sin2\theta\cos\theta$ tendency in V_L. As seen in Fig. 3(a), the $V_{AL}^0\sin2\theta\cos\theta$ function can fit the θ dependence of V_{AL} very well, although the present device does not have any conductive layers except for the Py. A possible source of τ_Y^0 will be discussed later. In contrast to V_{AL}, V_L is not fitted by

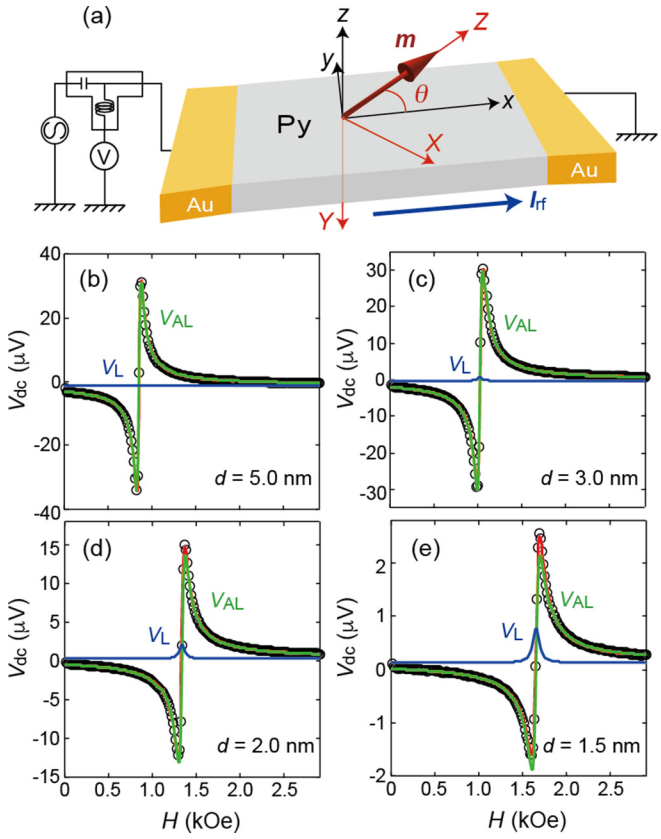

FIG. 2. (a) Illustration of device and measurement setup for spin-torque ferromagnetic resonance (ST-FMR) together with the coordinates. The ST-FMR spectra for (b) $d = 5.0$ nm, (c) $d = 3.0$ nm, (d) $d = 2.0$ nm, and (e) $d = 1.5$ nm. The frequency of radiofrequency current (f) was set to 7 GHz, and the external magnetic field (H) was applied at the in-plane angle (θ) of 45°. The blue and green curves represent the fitted results by Lorentzian (V_L) and anti-Lorentzian functions (V_{AL}), respectively, and red curves are the summations of V_L and V_{AL}.

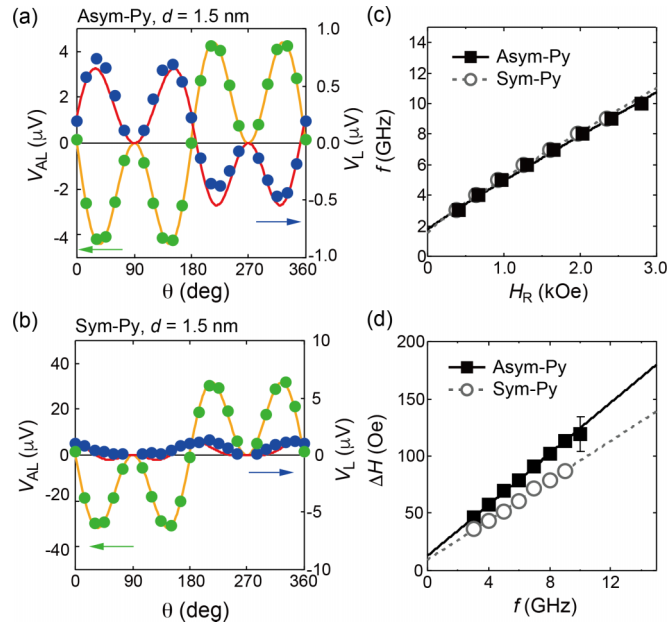

FIG. 3. The θ dependence of V_L (blue circles) and V_{AL} (green circles) for (a) Asym-Py with $d = 1.5$ nm and (b) Sym-Py with $d = 1.5$ nm, where the solid curves are the fitting results. (c) f vs resonance magnetic field (H_R) and (d) resonance linewidth (ΔH) vs f for Asym-Py (solid squares) and Sym-Py (open circles) with $d = 1.5$ nm, where the solid and dashed lines denote the fitting results.

the simple $\sin2\theta\cos\theta$ function (see Appendix A 1). This suggests that there exists an additional V_{dc} component. Previous papers [43,44] reported that the dynamic change in the AMR is given by $\Delta R \cdot m_x^2(t)$, and the time-averaged $m_x^2(t)$, i.e., $\langle m_x^2(t)\rangle$, leads to the modulation of DC resistance. As a result, the product of $\Delta R\langle m_x^2(t)\rangle$ and DC current (I_{dc}) leads to V_{dc}. Although we have not obtained clear experimental evidence, the Seebeck effect may be one of the possible sources for I_{dc}. For the present device, the RF power may heat the device locally and generate an in-plane thermal gradient along the $-x$ direction, resulting in an in-plane I_{dc} due to the Seebeck effect (for more details, see Appendix A 1). This $I_{dc}\Delta R\langle m_x^2(t)\rangle$ follows the $\cos^2\theta\cos2\theta$ function. Here, we should also mention that DC voltage generated by the existence of I_{dc} in the FMR spectra is similar to the microwave photoresistance phenomenon [45]. By taking into account this additional V_{dc}, the θ dependence of V_L is well fitted by $V_L^0\sin2\theta\cos\theta + V_L^{'}\cos^2\theta\cos2\theta$, and we find the remarkable V_L^0, indicating the existence of τ_X^0 for Asym-Py with $d = 1.5$ nm. Figure 3(b) shows the results for Sym-Py with $d = 1.5$ nm. As in the case of Asym-Py, τ_Y^0 appears. On the other hand, the V_L for Sym-Py involves only the $I_{dc}\Delta R\langle m_x^2(t)\rangle$ component, and τ_X^0 is not observed clearly. These are totally different from V_L for Asym-Py. In addition to the measurement at $f = 7$ GHz, the θ dependences of V_{AL} and V_L for Asym-Py and Sym-Py were investigated at $f = 5$ and 9 GHz, and similar angular dependences were observed, which are summarized in Appendix A 2.

Figure 3(c) plots the f vs H_R for Asym-Py and Sym-Py with $d = 1.5$ nm. It is confirmed that the experimental results obey the Kittel's equation of $f = (\gamma/2\pi)\sqrt{(H_R + H_{ani})(H_R + 4\pi M_{eff})}$, where γ is the gyromagnetic ratio, H_{ani} is the anisotropy field in the film plane, and $4\pi M_{eff}$ is the effective demagnetizing field. The values of H_{ani} and M_{eff} for all samples are discussed in Appendix A 3. Figure 3(d) shows ΔH as a function of f. The experimental data were fitted with $\Delta H = 4\pi f\alpha_0/\gamma + \Delta H_0$, where α_0 is the damping parameter. The values of α_0 and ΔH_0 for Asym-Py (Sym-Py) with $d = 1.5$ nm are obtained to be 0.0156 ± 0.0001 (0.0121 ± 0.0003) and 13 Oe (9 Oe), respectively. Figure 4(a) summarizes the d dependence of α_0. As d is reduced, one can see that α_0 is enhanced, particularly for Asym-Py. This fact means that the two different interfaces in the asymmetric structure give enhanced damping. At this moment, we consider that this enhancement comes from the inhomogeneity of magnetic properties in the thin Py layer sandwiched by the two different oxide layers.

Here, let us summarize the main features of ST-FMR for the Py single layer: (i) τ_Y^0 appears for both Asym-Py and Sym-Py, (ii) τ_X^0 is observed only for Asym-Py, (iii) τ_X^0 becomes remarkable as d is reduced, and (iv) Asym-Py exhibits the larger damping parameter than Sym-Py. First, we discuss the

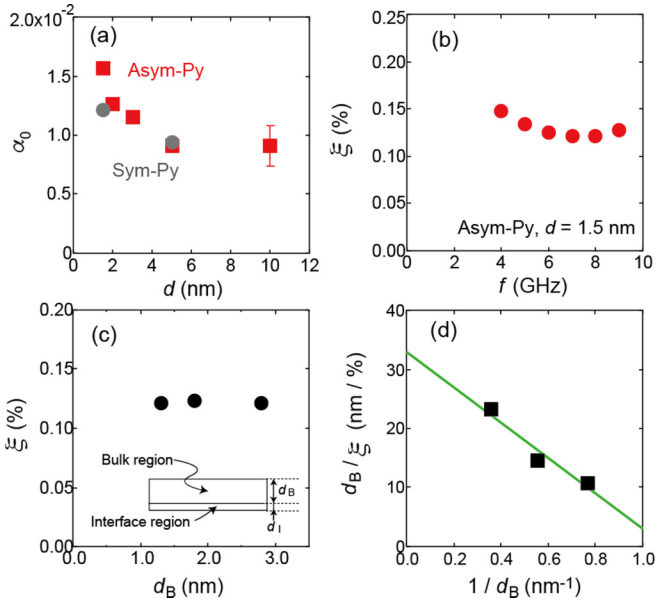

FIG. 4. (a) d dependence of magnetic damping constant (α_0), where the red squares and gray circles denote the data of Asym-Py and Sym-Py, respectively. (b) The parameter ξ as a function of f for Asym-Py with $d = 1.5$ nm with the assumption of the interface Py layer with $d_I = 0.2$ nm. (c) ξ as a function of the thickness of the bulk Py layer (d_B) and (d) d_B/ξ as a function of $1/d_B$ for Asym-Py at $f = 7$ GHz. The solid line in (d) represents the result of linear fitting. The inset of (c) illustrates the single layer consisting of bulk and interface regions.

source of τ_Y^0. According to the previous paper reporting on the interfacial spin-orbit coupling [46], the Rashba-Edelstein effect is a possible source of τ_Y^0. However, the fact that even Sym-Py shows the clear τ_Y^0 indicates that the Rashba-Edelstein effect may not be a major source of τ_Y^0 because the two identical interfaces ideally give no spin accumulation. Instead, we consider the possibility of the Oersted field because the imperfection of structure gives rise to the spatially inhomogeneous current distribution in the Py layer. For understanding the Oersted field generation, the ST-FMR was measured also for the Py/Pt reference samples, and at $\theta = 45°$, the positive (negative) V_L and negative (positive) V_{AL} were observed for the Subs.//Pt/Py (Subs.//Py/Pt) stack, as shown in Appendix A 4. Given the signs of V_{AL} for the reference samples, τ_Y^0 for both Asym-Py and Sym-Py is mainly attributable to the Oersted field originating from the electric current flowing at the bottom side of the Py layer. We highlight that V_{AL} of Asym-Py is nearly one order of magnitude smaller than that of Sym-Py. Meanwhile, ρ only increases by ~30%. One possibility is, for an unknown reason, the inhomogeneity of current distribution is more severe for Sym-Py. Another explanation is the contribution of fieldlike torque. If we assume the dissipated microwave power and current distribution of these structures are not very different, V_{AL} for Sym-Py is expected to become ~2.4 times larger than Asym-Py, which comes from the smaller ρ and larger AMR for Sym-Py (not shown here). This estimated V_{AL} cannot explain the dramatic change of V_{AL}. This could indicate the emergence of fieldlike torque that competes with the Oersted field when the stack is asymmetric. We will see later that this is consistent with the d dependence of ST-FMR.

In contrast to τ_Y^0 observed for both Asym-Py and Sym-Py, τ_X^0 is observed only for Asym-Py with $d \leqslant 3.0$ nm. This may be related to the enhanced α_0 for Asym-Py. A possible scenario to explain τ_X^0 is as follows: The magnetic properties are frequently modulated by contact with another material at the interface. In the case of Asym-Py, those properties could be modulated differently at the interfaces with Al-O and Si-O. As d is reduced, the spatial change of properties in one direction, which exists along the z direction in the present Py, becomes steep inside the Py because of the remarkable contribution of the interface effect. This unidirectional variation of the magnetic properties may generate the nonzero J_s via the SHE in Py and the resultant τ_X^0. Since Sym-Py ideally possesses two identical interfaces, on the other hand, the J_s due to the spatially changed magnetic property cancel out each other.

Hereafter, we quantitatively analyze the spin-torque efficiency of Py for Asym-Py. In order to extend the conventional analytical model used for a NM/FM bilayer [3] to self-induced SOT, we propose a toy model. In this toy model, there are two regions in the Py layer: the bulk and interface Py layers, as shown in the inset of Fig. 4(c). The resistivity and thickness of the bulk (interface) Py layer are denoted by ρ_B and d_B (ρ_I and d_I), respectively, and only the bulk Py layer has magnetization, while the interface Py layer has no magnetization because of the reduction of M_s with decreasing d, as shown in Fig. 1(d). Then we consider τ_Y^0 coming from the Oersted field and the interface effect such as the Rashba-Edelstein effect and τ_X^0 involving the bulk and interface contributions, which are represented by τ_X^B and τ_X^I, respectively. For the bulk contribution, it is assumed that the whole of the bulk layer generates J_s, and the resultant τ_X^B acts on the magnetic moments for the bulk layer itself. As in the case of the NM/FM bilayer, $V_L/V_{AL} = (\tau_X^0/\tau_Y^0)\sqrt{(H + H_{ani})/(H + 4\pi M_{eff})}$, and $\tau_X^0/\tau_Y^0 = \hbar(e\mu_0 M_s d_B d_I - \hbar\xi_{FL})^{-1}(\xi_{DL}^B \frac{\rho_I}{\rho_B} + \xi_{DL}^I)$, where $\hbar$ is the reduced Planck constant, e is the electric charge of an electron, μ_0 is the permeability in vacuum, ξ_{FL} is the fieldlike torque efficiency, ξ_{DL}^B is the dampinglike torque efficiency in the bulk Py layer, and ξ_{DL}^I is the efficiency of the dampinglike torque from the interface to the bulk Py layer (for detailed derivation, see Appendix A 5). Here, we introduce the parameter of ξ for convenience, which is $\xi \equiv (V_L/V_{AL}) \cdot (e\mu_0 M_s d_B^2/\hbar)\sqrt{(H + 4\pi M_{eff})/(H + H_{ani})}$. Although this parameter ξ has a form like the spin Hall angle for the NM/FM bilayer, it is noted that the ξ does not directly indicate the magnitude of self-induced SOT. Using the parameter ξ, the following relation between ξ_{DL}^B, ξ_{DL}^I, and ξ_{FL} is obtained:

$$\frac{1}{d_B}\xi = \left(\xi_{DL}^B \frac{\rho_I}{\rho_B} + \xi_{DL}^I\right) \Big/ \left\{ d_I \left(1 - \frac{\hbar\xi_{FL}}{e\mu_0 M_s d_B d_I}\right)\right\}. \quad (1)$$

Figure 4(b) plots the f dependence of ξ for $d = 1.5$ nm with the assumption of $d_I = 0.2$ nm. One sees that the values of ξ are in the range from 0.1 to 0.15% and do not depend on the frequency of I_{rf}. Here, ξ is almost constant irrespective of d_B, as shown in Fig. 4(c). Figure 4(d) shows d_B/ξ vs $1/d_B$. From the intercept of linear fit using Eq. (1), $\xi_{DL}^B \frac{\rho_I}{\rho_B} + \xi_{DL}^I$ ($= \xi_{DL}^{Total}$) was obtained to be 0.006%. In

addition to the evaluation by ST-FMR, we also carried out the harmonic Hall voltage measurement [4–8] and obtained the dampinglike torque efficiency of 0.04% (see Appendix A 6). Both the ST-FMR and the harmonic Hall voltage measurements gave small dampinglike torque efficiencies of the same sign. It is also worth mentioning that the slope of Fig. 4(d) is negative, indicating positive ξ_{FL}. This means that the positive fieldlike torque is opposing the Oersted field torque. In the current toy model, we focus on the total dampinglike torque efficiency instead of dampinglike torque efficiencies in the bulk Py layer and from the interface. At present, it is difficult to separately evaluate those dampinglike torque efficiencies with the independent control of interface SOT and bulk SOT. Our toy model provides one explanation to our experimental observations.

We make several remarks on our results. (i) We should mention the possibility of V_{dc} originating from the process of spin pumping and the following inverse SHE in Py. Although it is difficult to experimentally eliminate the influence of spin pumping from our ST-FMR result, the fact that the harmonic Hall voltage measurement also shows the small dampinglike torque efficiency implies that the spin pumping did not largely contribute to V_{dc} of ST-FMR. (ii) Also, $\xi_{\mathrm{DL}}^{\mathrm{Total}} = 0.006\%$ is two orders of magnitude smaller than the previously reported values such as 0.5% (Ref. [9]). For the present self-induced SOT experiment, the configuration between **m** and the spin angular momentum (**s**) of J_{s} is different from the previous experiments. If the spin anomalous Hall effect (SAHE) [12,17,22] is only the source of J_{s}, namely, the anomalous Hall current carries J_{s}, τ_X^0 is not given in the configuration of self-induced SOT because **m** is always parallel to **s**. On the other hand, if there exists a SHE showing the same symmetry as the SHE in NM, which is called M-independent SHE, that can provide the nonzero τ_X^0 acting on **m**. Our previous works [17,22] indicated that the negligibly small contribution of M-independent SHE exists. Thus, we consider that the small $\xi_{\mathrm{DL}}^{\mathrm{Total}}$ obtained by self-induced SOT comes from the M-independent SHE. Here, we mention that the sign of $\xi_{\mathrm{DL}}^{\mathrm{Total}}$ is the same as that of Pt with the assumption of J_{s} flowing along the $+z$ direction, which was also confirmed by the harmonic Hall voltage measurement (see Appendix A 6). (iii) Let us examine if such a small $\xi_{\mathrm{DL}}^{\mathrm{Total}}$ can drive the spin-torque auto-oscillation. According to Ref. [42], the spin Hall angle of ∼13% was required to reproduce the auto-oscillation in the nanoconstriction devices with the Py single layers capped with SiO_2. Thus, it seems hard to excite the auto-oscillation by using only self-induced SOT in the thin film form. However, since our results imply that the spatially nonuniform magnetic properties of Py provide nonnegligible τ_X^0, the nonuniform magnetization distribution in the vicinity of the constriction may lead to τ_X^0 sufficient for the auto-oscillation. (iv) We mention the important finding that the ST-FMR by self-induced SOT is a sensitive method for magnetic damping evaluation. As shown in Figs. 3(d) and 4(a), the determination of damping parameter with high accuracy was achieved even for the very thin Py layer with $d = 1.5$ nm. Therefore, we believe that this method will provide the fundamental knowledge of magnetization dynamics at the very small thickness region, which is essential for the development of spintronic devices requiring very thin FM layers.

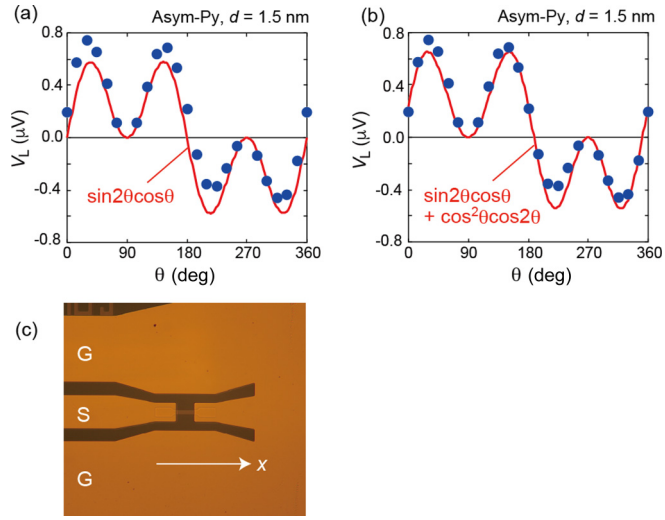

FIG. 5. In-plane angular dependence of V_{L} fitted with (a) the $\sin 2\theta\cos\theta$ function and (b) with the $\sin 2\theta\cos\theta + \cos^2\theta\cos 2\theta$ function. (c) Photograph of the present coplanar-waveguide-shaped device.

In conclusion, the self-induced SOT in the Py single layers was evaluated by using the ST-FMR technique. Employing Asym-Py and Sym-Py, we experimentally demonstrated the generation of τ_X^0 and τ_Y^0 in Py single-layer devices and discussed the possible scenario to explain the sources of τ_X^0 and τ_Y^0. We proposed a toy model to analyze self-induced SOT. This single-layer ST-FMR method is also beneficial for evaluating the magnetization dynamics for a very thin ferromagnetic layer.

The authors thank Y. Niimi for his valuable comments, R. Umetsu for her help in carrying out a part of the transport measurement, and T. Sasaki for her help in doing the film deposition by ion beam sputtering. The film deposition and device fabrication were carried out at the Cooperative Research and Development Center for Advanced Materials, IMR, Tohoku University. This paper was supported by JSPS KAKENHI Grant-in-Aid for Scientific Research (A) (JP20H00299), Grant-in-Aid for Scientific Research (S) (JP18H05246), and Grant-in-Aid for Early-Career Scientists (JP19K15430, JP20K15156).

APPENDIX

1. Details of fitting for angular dependence of V_{L}

As described in the main text, if τ_X^0 comes from the SHE, the combination of τ_{SH} and ΔR shows the $\sin 2\theta\cos\theta$ tendency in V_{L}. As shown in Fig. 5(a), however, the experimental data are not fitted well only by the $\sin 2\theta\cos\theta$ function. Particularly, the data at $\theta = 0$ and 180 ° show nonzero positive values, which cannot be fitted by the $\sin 2\theta\cos\theta$ function. Then we consider the following possibility. The dynamic change in the AMR is given by $\Delta R \cdot m_x^2(t)$, and $\langle m_x^2(t)\rangle$ leads to the change of DC resistance. Then if I_{dc} flows, the product of $\Delta R\langle m_x^2(t)\rangle$ and I_{dc} generates V_{dc}. We think that the Seebeck effect is one of the possible sources for I_{dc}, although no direct experimental evidence has been obtained yet. In this paper, we use the

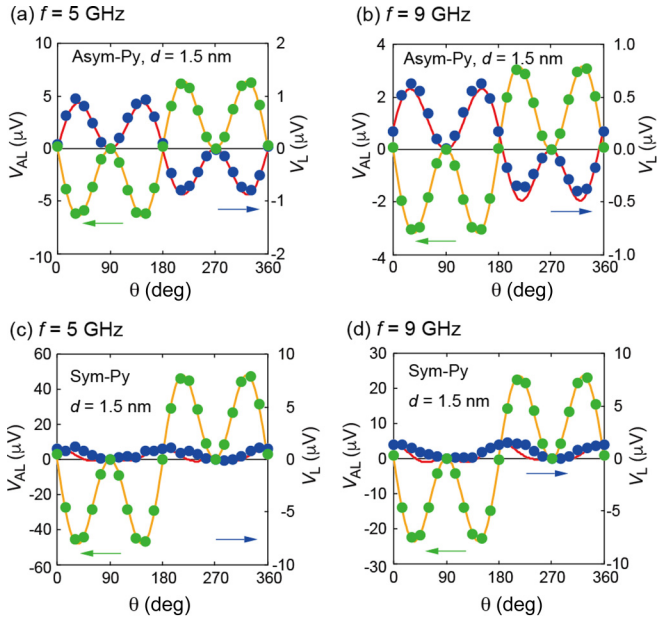

FIG. 6. The θ dependence of V_{L} (blue circles) and V_{AL} (green circles) for (a) Asym-Py at 5 GHz, (b) Asym-Py at 9 GHz, (c) Sym-Py at 5 GHz, and (d) Sym-Py at 9 GHz. The Py layer thickness was 1.5 nm. The solid curves are the fitting results.

coplanar-waveguide-shaped device, having the shorted end as seen in the photograph of Fig. 5(c). In the laterally asymmetric device structure with the narrow single (S) line and the wide ground (G) line, local heating occurs at the junction between the Py rectangular element and the Cr/Au electrode. This may give rise to a temperature gradient along the x direction and the resultant DC via the Seebeck effect. The V_{dc} due to the $\langle m_x^2(t)\rangle$ is given by $V_{\mathrm{dc}} = (\frac{1}{2})(\partial^2 V/\partial\theta^2)\,\langle\delta\theta(t)^2\rangle = -\Delta R\cos 2\theta\langle\delta\theta(t)^2\rangle$. Since $\langle\delta\theta(t)^2\rangle$ is proportional to $\cos^2\theta$, V_{dc} follows the $\cos^2\theta\cos 2\theta$ function. The result of fitting with $V_{\mathrm{L}}^0\sin 2\theta\cos\theta + V_{\mathrm{L}}^{'}\cos^2\theta\cos 2\theta$ is shown in Fig. 5(b).

2. Angular dependence of V_{AL} and V_{L} measured at different excitation frequencies

In addition to the measurement at $f = 7$ GHz shown in Figs. 3(a) and 3(b), the field angular dependence of the rectification voltage of ST-FMR was investigated at $f = 5$ and 9 GHz. Figures 6(a) and 6(b) show the θ dependences of V_{AL} and V_{L} for Asym-Py, whereas Figs. 6(c) and 6(d) show the results for Sym-Py. One sees that similar angular dependence was observed regardless of the excitation frequency.

3. H_{ani} and $\mathrm{M_{eff}}$ estimated from ST-FMR spectra

The plot of f vs H_{R} allows us to estimate H_{ani} in the film plane and the effective demagnetizing field of $4\pi M_{\mathrm{eff}}$ by using the Kittel's relationship. Figures 7(a) and 7(b) show the d dependence of H_{ani} and M_{eff}, respectively.

4. ST-FMR measurement for Py/Pt reference samples

In addition to the devices with the Py single layer, we carried out the ST-FMR measurement for the Py/Pt reference samples, which provides useful information about the sign

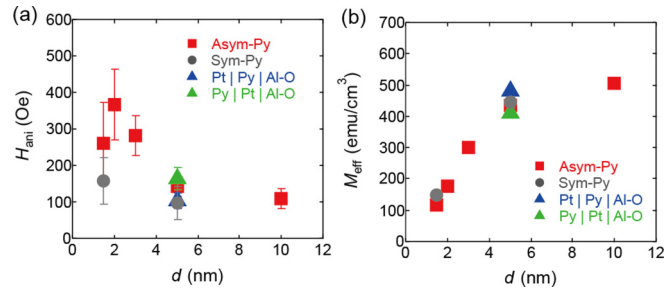

FIG. 7. (a) Py layer thickness (d) dependence of the anisotropy field (H_{ani}) and (b) effective magnetization (M_{eff}) for all the samples, which were obtained by the spin-torque ferromagnetic resonance (ST-FMR) measurement.

of τ_{SH} and the source of the Oersted field. Figures 8(a) and 8(b) display the ST-FMR spectra for the Subs.//Pt/Py and Subs.//Py/Pt stacks, respectively, measured at $\theta = 45\,^\circ$ and $f = 7$ GHz. The positive (negative) V_{L} and negative (positive) V_{AL} are observed for the Subs.//Pt/Py (Subs.//Py/Pt) stack. The θ dependences of V_{AL} and V_{L} for Subs.//Pt/Py and Subs.//Py/Pt are plotted in Figs. 8(c) and 8(d), respectively.

5. Toy model for analyzing SOT in a single ferromagnetic layer

We consider a single layer consisting of the bulk and the interface regions, as shown in the inset of Fig. 4(c), which are called the bulk Py layer and the interface Py layer, respectively. By using the resistivity and thickness of the bulk (interface) Py layer, which are denoted by ρ_{B} and d_{B} (ρ_{I} and d_{I}), respectively, and considering the parallel circuit, the

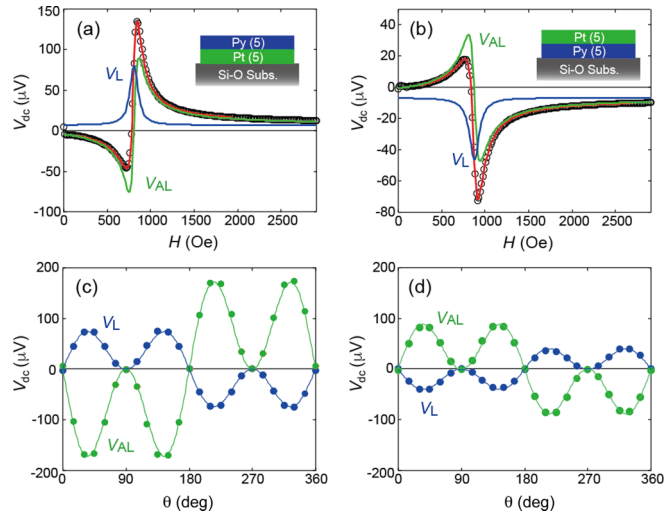

FIG. 8. (a) Spin-torque ferromagnetic resonance (ST-FMR) spectra and schematic illustration of the film stack for Subs.//Pt/Py and (b) Subs.//Py/Pt. The frequency of radiofrequency current (f) was set at 7 GHz, and the external magnetic field (H) was applied at the in-plane angle (θ) of 45 °. The blue and green curves represent the fitted results by Lorentzian (V_{L}) and anti-Lorentzian functions (V_{AL}), respectively, and red curves are the summations of V_{L} and V_{AL}. (c) The θ dependence of V_{L} (blue) and V_{AL} (green) for Subs.//Pt/Py and (d) Subs.//Py/Pt.

electric currents flowing in the bulk and interface Py layers, I_B and I_I, are given by

$$I_B = \frac{\frac{\rho_I}{d_I}}{\frac{\rho_B}{d_B}+\frac{\rho_I}{d_I}} I = \eta_B I, \tag{A1}$$

$$I_I = \frac{\frac{\rho_B}{d_B}}{\frac{\rho_B}{d_B}+\frac{\rho_I}{d_I}} I = \eta_I I, \tag{A2}$$

where η represents the ratio of current flow. It is assumed that only the bulk Py layer has magnetization, while the interface region has no magnetization.

The anti-Lorentzian component of ST-FMR spectra comes from τ_Y^0 including the Oersted field contribution and the interface effect such as the Rashba-Edelstein effect. The Oersted field torque (τ_Y^{Oe}) and the interface-induced fieldlike torque (τ_Y^{Inter}) are given by

$$\tau_Y^{Oe} = -\mu_0 \gamma \frac{\eta_I I_{rf}}{2w}, \tag{A3}$$

$$\tau_Y^{Inter} = \frac{\gamma \hbar \xi_{FL}}{2eM_s w d_I d_B} \eta_I I_{rf}, \tag{A4}$$

where w is the width of the coplanar waveguide.

In the present toy model, τ_X^0 involves two terms of bulk and interface contributions, which are represented by τ_X^B and τ_X^I, respectively. For the bulk contribution, it is assumed that the whole of the bulk Py layer generates J_s, and the resultant τ_X^B acts on the magnetic moments for the whole of the bulk Py layer. By using the ξ_{DL}^B, then τ_X^B is expressed as

$$\tau_X^B = -\frac{\gamma \hbar \xi_{DL}^B}{2eM_s w d_B^2} \eta_B I_{rf}. \tag{A5}$$

On the other hand, with ξ_{DL}^I, τ_X^I is given by

$$\tau_X^I = -\frac{\gamma \hbar \xi_{DL}^I}{2eM_s w d_I d_B} \eta_I I_{rf}. \tag{A6}$$

The ratio of V_L to V_{AL} is expressed as

$$\frac{V_L}{V_{AL}} = \sqrt{\frac{H+H_{ani}}{H+4\pi M_{eff}}} \frac{\tau_X^0}{\tau_Y^0}, \tag{A7}$$

which is transformed into

$$\frac{V_L}{V_{AL}} = \sqrt{\frac{H+H_{ani}}{H+4\pi M_{eff}}} \left(\frac{\hbar}{e\mu_0 M_s d_B d_I - \hbar \xi_{FL}}\right) \times \left(\xi_{DL}^B \frac{d_I}{d_B}\frac{\eta_B}{\eta_I} + \xi_{DL}^I\right). \tag{A8}$$

Then

$$\left(\xi_{DL}^B \frac{d_I}{d_B}\frac{\eta_B}{\eta_I} + \xi_{DL}^I\right) = \frac{V_L}{V_{AL}} \sqrt{\frac{H+4\pi M_{eff}}{H+H_{ani}}} \times \left(\frac{1}{\hbar} e\mu_0 M_s d_B d_I - \xi_{FL}\right), \tag{A9}$$

is obtained. Here, we put the parameter of ξ to be

$$\xi \equiv \frac{V_L}{V_{AL}} \frac{e\mu_0 M_s d_B^2}{\hbar} \sqrt{\frac{H+4\pi M_{eff}}{H+H_{ani}}}. \tag{A10}$$

Using ξ, Eq. (A9) can be rewritten into

$$\left(\xi_{DL}^B \frac{d_I}{d_B}\frac{\eta_B}{\eta_I} + \xi_{DL}^I\right) = \xi\left(1 - \frac{\hbar \xi_{FL}}{e\mu_0 M_s d_B d_I}\right)\frac{d_I}{d_B}. \tag{A11}$$

Since $d_I \eta_B / d_B \eta_I = \rho_I / \rho_B$, Eq. (A11) can be transformed into

$$\frac{1}{d_B}\xi = \frac{\xi_{DL}^B \frac{\rho_I}{\rho_B} + \xi_{DL}^I}{d_I\left(1 - \frac{\hbar \xi_{FL}}{e\mu_0 M_s d_B d_I}\right)}. \tag{A12}$$

Finally, the following relation between ξ and d_B is obtained:

$$\frac{d_B}{\xi} = a - \frac{1}{d_B} b, \tag{A13}$$

in which $a = d_I(\xi_{DL}^B \frac{\rho_I}{\rho_B} + \xi_{DL}^I)^{-1}$. Therefore, from the linear fit to the plot of d/ξ vs $1/d$, the total dampinglike torque efficiency coming from both the bulk and the interface can be evaluated by assuming the interface region with d_I.

6. Harmonic Hall voltage measurement for Asym-Py

Harmonic Hall voltage measurement [6] was carried out as an independent alternative for quantifying the spin-orbit effective fields in in-plane magnetized Asym-Py with $d = 1.5$ nm. A sinusoidal current excitation $I_0 \sin(\omega t)$ where $I_0 = 1.5$ mA and $\frac{\omega}{2\pi} = 172.1$ Hz was applied using an alternating current source meter along a micron-sized Hall bar device, while the first (R_ω) and second harmonic ($R_{2\omega}$) Hall resistances were simultaneously measured using two lock-in amplifiers. Here, H was applied and rotated within the film plane, making an azimuthal field angle (θ) with the current. Including thermoelectric contributions, R_ω and $R_{2\omega}$ can be described by the following equations:

$$R_\omega = R_{PHE} \sin 2\theta, \tag{A14}$$

$$R_{2\omega} = \left(R_{AHE}\frac{H_{DL}}{H_k + H} + R_{const}\right)\cos\theta - \left(2R_{PHE}\frac{H_{FL+Oe}}{H_{ani}+H}\right)\cos 2\theta \cos\theta = A\cos\theta + B\cos 2\theta \cos\theta, \tag{A15}$$

where R_{AHE} is the anomalous Hall resistance, R_{PHE} the planar Hall resistance, R_{const} the $R_{2\omega}$ component that does not depend on H, H_k the out-of-plane anisotropy field, H_{DL} the dampinglike spin-orbit effective field, and H_{FL+Oe} the fieldlike spin-orbit effective field including the Oersted field.

The θ angle dependence of $R_{2\omega}$ measured for various H ranging from 1 to 30 kOe is plotted in Figs. 9(a)–9(d). All data are well fitted using Eq. (A15), and the fitted curves can be decomposed into the sum of a $\cos\theta$ component (prefactor A; blue lines) and a $\cos 2\theta \cos\theta$ component (prefactor B; green lines). We should note that the change in the angular

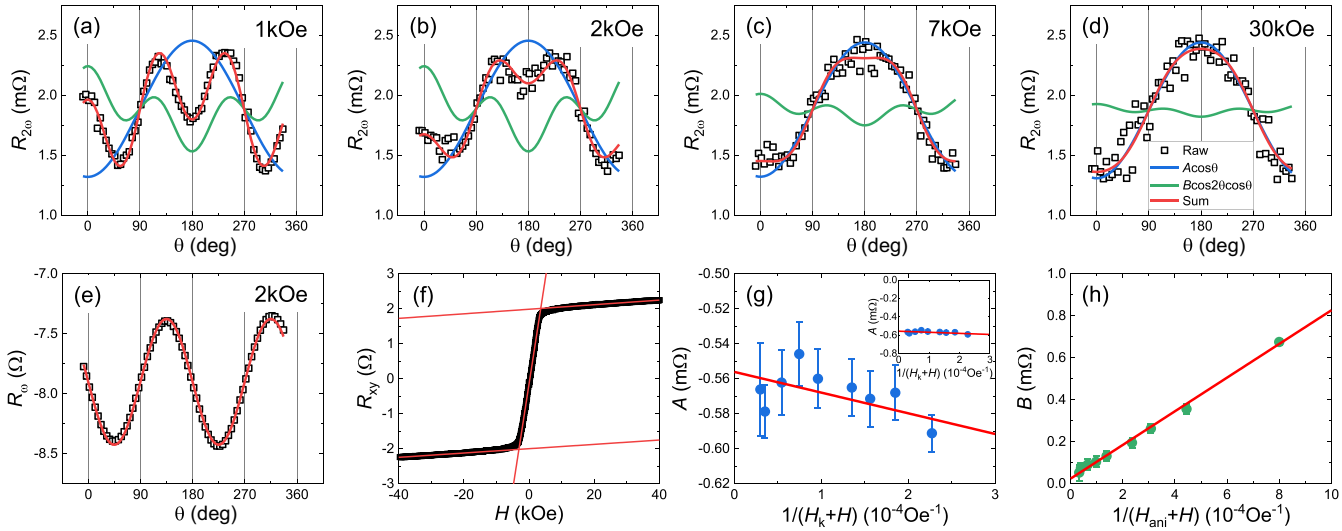

FIG. 9. Azimuthal field angle θ dependence of second harmonic Hall resistance $R_{2\omega}$ for Asym-Py ($d = 1.5$ nm) at various external fields: (a) $H = 1$ kOe, (b) $H = 2$ kOe, (c) $H = 7$ kOe, and (d) $H = 30$ kOe. Red lines are fits to the raw data (open black squares) using Eq. (A15). Blue and green lines denote the decomposition of the $\cos\theta$ component (A) and $\cos 2\theta \cos\theta$ component (B), respectively. (e) θ dependence of the first harmonic Hall resistance R_ω for $H = 2$ kOe with best fit using Eq. (A14) (red line). (f) Transverse Hall resistance R_{xy} loop of the same Hall bar device measured with an applied field along the out-of-plane direction. (g) Prefactor A of the $\cos\theta$ component and (h) prefactor B of the $\cos 2\theta \cos\theta$ component against $1/(H_k + H)$ and $1/(H_{ani} + H)$, respectively. Red lines are best linear fits to the entire dataset. Inset of (g) shows the full y scale of the same data, reflecting A mainly consists of $R_{2\omega}$ contributions that do not depend on H.

dependence of $R_{2\omega}$ upon varying H is mainly due to changes in B, whereas A remains nearly constant. A typical θ angle dependence of R_ω for $H = 2$ kOe is shown in Fig. 9(e). Here, R_{PHE} is obtained from the fit by Eq. (A14). The anomalous Hall effect loop measured with an applied out-of-plane field is shown in Fig. 9(f). Upon eliminating the ordinary Hall effect contribution by linearly fitting the data points at high fields, we extract $R_{AHE} \sim 2\ \Omega$ and $H_k \sim 3400$ Oe. Note that the sign of the R_{AHE} contribution of this ultrathin Asym-Py is the same as Ni and is opposite to Co and Fe, which is consistent with previous work [25]. Using $H_{ani} \sim 250$ Oe obtained from Fig. 7, A and B are plotted against $1/(H_k + H)$ and $1/(H_{ani} + H)$, respectively, in Figs. 9(g) and 9(h). Here, $H_{DL} \sim 0.06$ Oe and $H_{FL+Oe} \sim 0.75$ Oe are extracted from the linear fits to these plots. Assuming uniform current distribution, for $I_0 = 1.5$ mA and $d = 1.5$ nm, we obtain a lower bound of the current density $j = 1.0 \times 10^7$ A cm^{-2}. Using this j, we can estimate an upper bound of the dampinglike spin Hall efficiency ξ_{DL}:

$$\xi_{DL} = \frac{2e}{\hbar}\frac{H_{DL} M_s d}{j}. \tag{A16}$$

If we consider that a net spin current is generated from the bottom interface of the Py and acts on the entire magnetic film, we obtain a relatively small $\xi_{DL} \approx 0.015\%$, which is equivalent to a spin Hall layer underneath Py with a positive spin Hall angle (same as Pt). These agree with the ST-FMR. We emphasize that the accuracy of this measurement is limited because A is dominated by the R_{const} contribution at the y intercept, as shown in the inset of Fig. 9(g). Our results also demonstrate the necessity of measuring the H dependence of $R_{2\omega}(\theta)$ for correctly evaluating the self ξ_{DL} of Asym-Py. The H_{FL+Oe} extracted from the harmonic Hall voltage measurement is of the same order as the expected Oersted field generated by Asym-Py on applying j.

[1] A. Hoffman, IEEE Trans. Magn. **49**, 5172 (2013).

[2] X. Han, X. Wang, C. Wan, G. Yu, and X. Lv, Appl. Phys. Lett. **118**, 120502 (2021).

[3] L. Liu, T. Moriyama, D. C. Ralph, and R. A. Buhrman, Phys. Rev. Lett. **106**, 036601 (2011).

[4] K. Garello, I. M. Miron, C. O. Avci, F. Freimuth, Y. Mokrousov, S. Blügel, S. Auffret, O. Boulle, G. Gaudin, and P. Gambardella, Nat. Nanotechnol. **8**, 587 (2013).

[5] J. Kim, J. Sinha, M. Hayashi, M. Yamanouchi, S. Fukami, T. Suzuki, S. Mitani, and H. Ohno, Nat. Mater. **12**, 240 (2013).

[6] C. O. Avci, K. Garello, M. Gabureac, A. Ghosh, A. Fuhrer, S. F. Alvarado, and P. Gambardella, Phys. Rev. B **90**, 224427 (2014).

[7] Y.-C. Lau and M. Hayashi, Jpn. J. Appl. Phys. **56**, 0802B5 (2017).

[8] H. Masuda, R. Modak, T. Seki, K. Uchida, Y.-C. Lau, Y. Sakuraba, R. Iguchi, and K. Takanashi, Commun. Mater. **1**, 75 (2020).

[9] B. F. Miao, S. Y. Huang, D. Qu, and C. L. Chien, Phys. Rev. Lett. **111**, 066602 (2013).

[10] S. M. Wu, J. Hoffman, J. E. Pearson, and A. Bhattacharya, Appl. Phys. Lett. **105**, 092409 (2014).

[11] T. Seki, K. Uchida, T. Kikkawa, Z. Qiu, E. Saitoh, and K. Takanashi, Appl. Phys. Lett. **107**, 092401 (2015).

[12] T. Taniguchi, J. Grollier, and M. D. Stiles, Phys. Rev. Appl. **3**, 044001 (2015).

[13] D. Tian, Y. Li, D. Qu, S. Y. Huang, X. Jin, and C. L. Chien, Phys. Rev. B **94**, 020403(R) (2016).
[14] V. P. Amin and M. D. Stiles, Phys. Rev. B **94**, 104419 (2016).
[15] C. Qin, S. Chen, Y. Cai, F. Kandaz, and Y. Ji, Phys. Rev. B **96**, 134418 (2017).
[16] K. S. Das, W. Y. Schoemaker, B. J. van Wees, and I. J. Vera-Marun, Phys. Rev. B **96**, 220408(R) (2017).
[17] S. Iihama, T. Taniguchi, K. Yakushiji, A. Fukushima, Y. Shiota, S. Tsunegi, R. Hiramatsu, S. Yuasa, Y. Suzuki, and H. Kubota, Nat. Electron. **1**, 120 (2018).
[18] J. D. Gibbons, D. MacNeill, R. A. Buhrman, and D. C. Ralph, Phys. Rev. Appl. **9**, 064033 (2018).
[19] A. Bose, D. D. Lam, S. Bhuktare, S. Dutta, H. Singh, Y. Jibiki, M. Goto, S. Miwa, and A. A. Tulapurkar, Phys. Rev. Appl. **9**, 064026 (2018).
[20] S. C. Baek, V. P. Amin, Y. W. Oh, G. Go, S. J. Lee, G. H. Lee, K. J. Kim, M. D. Stiles, B. G. Park, and K. J. Lee, Nature Mater. **17**, 509 (2018).
[21] J. Cramer, A. Ross, S. Jaiswal, L. Baldrati, R. Lebrun, and M. Kläui, Phys. Rev. B **99**, 104414 (2019).
[22] T. Seki, S. Iihama, T. Taniguchi, and K. Takanashi, Phys. Rev. B **100**, 144427 (2019).
[23] Z. Wen, Z. Qiu, S. Tölle, C. Gorini, T. Seki, D. Hou, T. Kubota, U. Eckern, E. Saitoh, and K. Takanashi, Sci. Adv. **5**, eaaw9337 (2019).
[24] C. Safranski, E. A. Montoya, and I. N. Krivorotov, Nat. Nanotechnol. **14**, 27 (2019).
[25] Y. Omori, E. Sagasta, Y. Niimi, M. Gradhand, L. E. Hueso, F. Casanova, and Y. Otani, Phys. Rev. B **99**, 014403 (2019).
[26] Y. Hibino, K. Hasegawa, T. Koyama, and D. Chiba, APL Mater. **8**, 041110 (2020).
[27] Y. Hibino, K. Yakushiji, A. Fukushima, H. Kubota, and S. Yuasa, Phys. Rev. B **101**, 174441 (2020).
[28] A. Yagmur, S. Sumi, H. Awano, and K. Tanabe, Phys. Rev. Appl. **14**, 064025 (2020).
[29] Y. Koike, S. Iihama, and S. Mizukami, Jpn. J. Appl. Phys. **59**, 090907 (2020).
[30] K. Tang, Z. Wen, Y.-C. Lau, H. Sukegawa, T. Seki, and S. Mitani, Appl. Phys. Lett. **118**, 062402 (2021).
[31] L. Leiva, S. Granville, Y. Zhang, S. Dushenko, E. Shigematsu, T. Shinjo, R. Ohshima, Y. Ando, and M. Shiraishi, Phys. Rev. B **103**, L041114 (2021).
[32] L. Liu, J. Yu, R. González-Hernández, C. Li, J. Deng, W. Lin, C. Zhou, T. Zhou, J. Zhou, H. Wang, R. Guo, H. Y. Yoong, G. M. Chow, X. Han, B. Dupé, J. Železnyé, J. Sinova, and J. Chen, Phys. Rev. B **101**, 220402(R) (2020).
[33] M. Tang, K. Shen, S. Xu, H. Yang, S. Hu, W. Luü, C. Li, M. Li, Z. Yuan, S. J. Pennycook, K. Xia, A. Manchon, S. Zhou, and X. Qiu, Adv. Mater. **32**, 2002607 (2020).
[34] T. Sato, T. Seki, M. Kohda, J. Ryu, H. Gamou, S. Karube, K. Takanashi, and J. Nitta, Jpn. J. Appl. Phys. **58**, 060915 (2019).
[35] S. Q. Zheng, K. K. Meng, Q. B. Liu, J. K. Chen, J. Miao, X. G. Xu, and Y. Jiang, Appl. Phys. Lett. **117**, 242403 (2020).
[36] L. Zhu, X. S. Zhang, D. A. Muller, D. C. Ralph, and R. A. Buhrman, Adv. Funct. Mater. **30**, 2005201 (2020).
[37] Z. Chen, L. Liu, Z. Ye, Z. Chen, H. Zheng, W. Jia, Q. Zeng, N. Wang, B. Xiang, T. Lin, J. Liu, M. Qiu, S. Li, J. Shi, P. Han, and H. An, Appl. Phys. Exp. **14**, 033002 (2021).
[38] Y. Yang, Z. Luo, H. Wu, Y. Xu, R.-W. Li, S. J. Pennycook, S. Zhang, and Y. Wu, Nat. Commun. **9**, 2255 (2018).
[39] Z. Luo, Q. Zhang, Y. Xu, Y. Yang, X. Zhang, and Y. Wu, Phys. Rev. Appl. **11**, 064021 (2019).
[40] J. W. Lee, J. Y. Park, J. M. Yuk, and B.-G. Park, Phys. Rev. Appl. **13**, 044030 (2020).
[41] W. Wang, T. Wang, V. P. Amin, Y. Wang, A. Radhakrishnan, A. Davidson, S. R. Allen, T. J. Silva, H. Ohldag, D. Balzar, B. L. Zink, P. M. Haney, J. Q. Xiao, D. G. Cahill, V. O. Lorenz, and X. Fan, Nat. Nanotechnol. **14**, 819 (2019).
[42] M. Haidar, A. A. Awad, M. Dvornik, R. Khymyn, A. Houshang, and J. Åkerman, Nat. Commun. **10**, 2362 (2019).
[43] M. V. Costache, S. M. Watts, M. Sladkov, C. H. van der Wal, and B. J. van Wees, Appl. Phys. Lett. **89**, 232115 (2006).
[44] S. Hirayama, S. Mitani, Y. Otani, and S. Kasai, Jpn. J. Appl. Phys. **57**, 060301 (2018).
[45] N. Mecking, Y. S. Gui, and C.-M. Hu, Phys. Rev. B **76**, 224430 (2007).
[46] S. Emori, T. Nan, A. M. Belkessam, X. Wang, A. D. Matyushov, C. J. Babroski, Y. Gao, H. Lin, and N. X. Sun, Phys. Rev. B **93**, 180402(R) (2016).